

FLIGHT-MEASURED AERODYNAMIC LOADS  
ON A 0.92 ASPECT RATIO LIFTING SURFACE

Robert R. Meyer, Jr. and V. Michael DeAngelis  
Dryden Flight Research Center

SUMMARY

Ventral fin loads, expressed as normal force coefficients, bending moment coefficients, and torque coefficients, were measured during flight tests of a YF-12A airplane. Because of the proximity of the ventral fin to the ailerons, the aerodynamic loads presented were the result of both sideslip loads and aileron crossflow loads. Aerodynamic data obtained from strain gage loads instrumentation and some flight pressure measurements are presented for several Mach numbers ranging from 0.70 to 2.00. Selected wind tunnel data and results of linear theoretical aerodynamic calculations are presented for comparison.

INTRODUCTION

Because of their lower aerodynamic drag, low-aspect-ratio lifting surfaces are becoming more prevalent in high-speed aircraft designs. Typical examples are the low-aspect-ratio stabilizing surfaces used on both the XB-70 and YF-12 airplanes. Literature searches revealed very little experimental data to support recent advances in theoretical methods for predicting aerodynamic loads on very low-aspect-ratio lifting surfaces. References 1 to 3 present flight-measured aerodynamic loads data on the low-aspect-ratio lifting surfaces of trapezoidal planforms shown in figure 1. Of these three lifting surfaces, the XB-70 canard has the lowest aspect ratio at 1.65. For comparison, the YF-12 ventral fin with a 0.92 aspect ratio is also shown.

The change in lift curve slope and chordwise center-of-pressure location with Mach number is shown in figure 2 for the four planforms presented in figure 1. The three planforms with aspect ratios greater than 1.5 have similar characteristics in terms of the magnitude of the lift curve slope, the chordwise center-of-pressure location, and the variation of these two parameters with Mach number. However, for Mach numbers in the transonic region, the YF-12 ventral fin with an aspect ratio less than 1 shows distinct differences in the magnitude of the lift curve slope and

in the location of the chordwise center of pressure. Because the YF-12 ventral fin data differed significantly from data on the planforms with aspect ratios greater than 1.5, the centerline ventral fin of the YF-12A airplane was studied to add to the available data on low-aspect-ratio lifting surfaces at transonic speeds where the aerodynamic loads tend to be most severe.

The YF-12 ventral fin structure was found to be very rigid during ground tests and was considered to remain rigid throughout the flight envelope investigated. This rigidity made the flight data obtained from the ventral fin ideal for comparison with wind tunnel data and with theoretical aerodynamic calculations for rigid structures.

Aerodynamic data obtained from strain gage loads instrumentation and some flight pressure measurements are presented for several Mach numbers ranging from 0.70 to 2.00. Selected wind tunnel data and results from theoretical aerodynamic calculations are presented for comparison. Because of the proximity of the ventral fin to the ailerons, the measured aerodynamic loads resulted from a combination of sideslip loads and aileron crossflow loads.

## SYMBOLS

Physical quantities in this report are given in the International System of Units (SI). The measurements were taken and calculations were made in U.S. Customary Units. Factors relating the two systems are presented in reference 4.

The results of this investigation were derived from data obtained using the reference ventral-fin-panel planform defined in figure 3. The bending moment reference axis is the strain gage instrumentation axis. This axis is located at the 62.62-centimeter ventral fin station and is oriented normal to the 69.5-percent chord line. For clarification, the reference dimensions and areas used to nondimensionalize the flight data are included in the symbols list.

$B$	reference ventral fin bending moment, m-N
$b/2$	reference ventral fin semispan measured from the strain gage instrumentation station, 135.5 cm
$C_B$	aerodynamic bending moment coefficient of the reference ventral fin, $\frac{B}{qSb/2}$
$C_{B_\beta}$	$= \frac{\partial C_B}{\partial \beta}, \text{ per deg}$
$C_{B_{\delta_a}}$	$= \frac{\partial C_B}{\partial \delta_a}, \text{ per deg}$
$C_L$	lift coefficient, $\frac{L}{qS}$

$C_{L_\alpha}$	$= \frac{\partial C_L}{\partial \alpha}$ , per deg
$C_N$	aerodynamic normal force coefficient of the reference ventral fin, $\frac{N}{qS}$
$C_{N_\beta}$	$= \frac{\partial C_N}{\partial \beta}$ , per deg
$C_{N_{\delta_a}}$	$= \frac{\partial C_N}{\partial \delta_a}$ , per deg
$\Delta C_p$	differential pressure coefficient, $\frac{p_l - p_r}{q}$
$C_T$	aerodynamic torque coefficient of the reference ventral fin, $\frac{T}{qS\bar{c}}$
$C_{T_\beta}$	$= \frac{\partial C_T}{\partial \beta}$ , per deg
$C_{T_{\delta_a}}$	$= \frac{\partial C_T}{\partial \delta_a}$ , per deg
$c$	reference ventral fin local chord, cm
$\bar{c}$	reference ventral fin mean aerodynamic chord measured normal to 69.5-percent chord at ventral station 125.48 cm, 299.59 cm
$M$	Mach number
MAC	mean aerodynamic chord
$N$	reference ventral fin aerodynamic normal force, N
$p_l$	local static pressure on left surface of ventral fin, $N/m^2$
$p_r$	local static pressure on right surface of ventral fin, $N/m^2$
$q$	free stream dynamic pressure, $N/m^2$
$S$	reference ventral fin area, $4.00 m^2$
$T$	reference ventral fin torque, m-N
$x$	chordwise distance rearward of leading edge of local chord, cm

$\left(\frac{x}{c}\right)_{cp}$	reference ventral fin chordwise center of pressure location,	$\frac{C_{T\beta}}{C_{N\beta}}$
$\left(\frac{2y}{b}\right)_{cp}$	reference ventral fin spanwise center of pressure location,	$\frac{C_{B\beta}}{C_{N\beta}}$
$\alpha$	airplane angle of attack, deg	
$\beta$	airplane angle of sideslip, deg	
$\delta_a$	differential aileron deflection, left aileron position minus right aileron position, deg	

### FLIGHT TEST VENTRAL FIN DESCRIPTION

The ventral fin, located on the aft fuselage of the YF-12A aircraft (fig. 4), is hinged along the root axis at the front spar (40-percent chord) and at the aft spar (75-percent chord) and is folded parallel to the wing for takeoff and landing clearance. The fin, which incorporates a hexagonal airfoil shape with a thickness-to-chord ratio of 0.03, was designed to increase lateral-directional stability at high speeds. The 4.0-m<sup>2</sup> area is based on the defined ventral-fin-panel planform, with an aspect ratio of 0.92 (fig. 3). As shown in figure 4, the ventral fin is located near the inboard ailerons where it is subject to loads induced by the differential deflection of the ailerons.

The substructure of the ventral fin is constructed of titanium. The leading and trailing edges and the skin panels are constructed from a beryllium-aluminum alloy. The stiffness of the fin, determined from static loadings, precluded measuring any aeroelastic effects throughout the flight envelope investigated.

### FLIGHT INSTRUMENTATION AND ACCURACIES

The ventral fin was instrumented with strain gages located at its root and with four chordwise rows of static pressure orifices. To measure shear or normal force, bending moment, and torque on the ventral fin, the strain gages were calibrated using the method described in reference 5. Most of the static pressure orifices were holes drilled through the center of skin fasteners, with the exception of the leading edge orifices which were holes drilled in the leading edge. Two types of pressure sensing instrumentation were used. The first type, intended to obtain data only during steady-state flight maneuvers, was scanning valves plumbed to chordwise pressure orifice rows at the 93.98-centimeter, 119.18-centimeter, and 173.48-centimeter ventral stations. The second type, intended to obtain data during both steady-state and dynamic flight maneuvers, was individual pressure transducers plumbed to a chordwise pressure orifice row at the 144.53-centimeter ventral station. The location of the pressure orifices and strain gage instrumentation is shown in figure 5.

The measurement of aircraft parameters such as Mach number, angle of attack, and angle of sideslip have been documented in other reports, such as reference 6. The estimated accuracies of all measured quantities used in this report are presented in table 1.

## WIND TUNNEL TESTS

Transonic pressure measurements were obtained from tests of the 1/12-scale sting-mounted model of the YF-12A airplane in the NASA Ames 11-Foot Wind Tunnel. The wind tunnel model ventral fin was instrumented with four chordwise rows of static pressure orifices which corresponded closely to the relative locations of the pressure orifices on the ventral fin of the flight vehicle. Most of the pressure data were obtained at a Reynolds number of  $7.62 \times 10^6$  per meter, and a few selected points were run at a Reynolds number of  $20.32 \times 10^6$  per meter. Since no apparent differences were noted in the data, the wind tunnel data obtained at the lower Reynolds number were used. These data were integrated to obtain the ventral fin aerodynamic loads.

## THEORETICAL ANALYSIS

The theoretical data were obtained from the FLEXSTAB computer program (ref. 7). FLEXSTAB is a system of digital computer programs based on linear theories for evaluating the static and dynamic stability, trim state, structural loading, and elastic deformations of arbitrary aircraft configurations in subsonic and supersonic flight. The linear aerodynamic analytical method used in FLEXSTAB is essentially that developed by Woodward (refs. 8 and 9) for representing supersonic flow about wing-body combinations. The method has been extended to include subsonic flow with arbitrary wing-body, nacelle, and tail arrangements.

When using the FLEXSTAB program to calculate the ventral fin loads, no attempt was made to incorporate boundary layer effects. Since ground static loadings showed the ventral fin to be very rigid, all theoretical aerodynamic data presented for comparison with flight-measured data and wind tunnel data are for a rigid fin configuration.

## RESULTS AND DISCUSSION

The flight loads were obtained from two types of maneuvers: (1) a dynamic aileron pulse maneuver which imposed essentially pure aileron crossflow loads on the fin, and (2) a steady-sideslip maneuver which imposed a combination of sideslip and aileron crossflow loads on the fin. Pressure load distributions of wind tunnel aileron crossflow loads and flight-derived steady-sideslip loads for a Mach number of 0.90 are presented in figures 6 and 7, respectively.

Figure 6 presents a representative wind tunnel pressure load distribution due to aileron deflection along the four chordwise rows of pressure orifices. It appears

that the effect of aileron deflection on bending moment is negligible because the load is concentrated at the root of the fin. However, the torque load is notable due to the long moment arm about the quarter chord point of the MAC. In this case the load is concentrated toward the trailing edge of the ventral fin from about 70 percent to 100 percent of the MAC depending on Mach number.

Figure 7 shows a flight ventral fin pressure distribution during a steady-state sideslip maneuver. It suggests that the increase in angle of sideslip loads the leading edge of the fin while the aileron deflection loads the aft portion of the fin in the opposite direction. While this combination tends to cancel normal and bending moment loads, it tends to increase torque loads about the quarter chord point of the MAC. This could cause an excessive torque load during certain flight conditions. Figure 7 shows the differential surface pressures,  $\Delta C_p$ . For the flight condition presented, the  $\Delta C_p$  distribution in the vicinity of the leading edge is representative of the distribution of the pressures on the surface with the low pressure field. Therefore, the high leading edge pressures of rows 2, 3, and 4, followed by the large pressure gradient, suggest that a leading edge vortex is present.

Figure 8 presents flight-measured aerodynamic normal force coefficient data, bending moment coefficient data, and torque coefficient data plotted against angle of sideslip. These data are compared with wind tunnel measurements and theoretical calculations for a Mach number of 0.90. The flight data were obtained from the strain gage loads instrumentation during steady sideslip maneuvers and were corrected for the presence of the aileron crossflow loads by subtracting the aileron crossflow component loads ( $C_{N_{\delta_a}}$ ,  $C_{B_{\delta_a}}$ , and  $C_{T_{\delta_a}}$ ) which were determined from the aileron pulse maneuvers. A least-squares straight line was fitted to the wind tunnel data for the data points above  $-2^\circ$  angle of sideslip. It was felt that below  $-2^\circ$  angle of sideslip, the leading edge vortex would affect the linearity of the curve. From the  $C_N$  and  $C_B$  data for  $-5^\circ$  and  $-6^\circ$  angle of sideslip, the presence of a leading edge vortex condition appears to have influenced the integrated pressure data. By indicating a decrease in torque at the lower sideslip angles, the  $C_T$  data do not appear to substantiate the vortex effects shown by the  $C_N$  and  $C_B$  data. However, because of the leading edge sweep and the idealized geometric planform shape, and because the effect of the vortex seems to be most pronounced at the outboard rows of pressure orifices, the effect of the vortex should be more pronounced on the integrated coefficients of  $C_N$  and  $C_B$  than on  $C_T$ . Also, since the large pressure gradients at the leading edge are defined by only a few pressure orifices, the effect of the leading edge vortex on the  $C_T$  data is probably lost in the resolution of the data and in the mechanics of the integration. The theoretical calculations are based on linear theory and do not account for the presence of a leading edge vortex.

Slopes were obtained from the data presented in figure 8 and from similar data obtained at other Mach numbers. These computations presented in figure 9 show the normal force coefficient slopes as well as the spanwise and chordwise center-of-pressure locations. The flight-derived  $C_{N_\beta}$  data show that the maximum value of

$C_{N\beta}$  occurs at low supersonic speeds around Mach 1.2 to Mach 1.4. The wind tunnel  $C_{N\beta}$  data agree with the flight data at Mach 0.70 and Mach 0.90, but underpredict the normal force curve slope at Mach 0.95. The disagreement at Mach 0.95 may be due to the problem of defining the large leading edge pressure gradient with only a few pressure orifices. The theoretical calculations show similar trends in the variation of  $C_{N\beta}$  with Mach number, but slightly underpredict  $C_{N\beta}$  at transonic speeds.

At transonic conditions the strain gage flight-measured spanwise center-of-pressure locations vary from 52 percent to 58 percent of the semispan. The wind tunnel data and theoretical calculations place the spanwise center-of-pressure location between 42 percent and 48 percent of the semispan. At supersonic conditions, the flight-measured spanwise center of pressure shifts substantially inboard.

An analysis of the strain gage calibration data indicates that a larger than actual bending moment is obtained from the bending moment equation when the load is applied to the leading edge of the ventral fin, and a smaller than actual bending moment is obtained from the bending moment equation when the load is applied to the center and aft portions of the fin. Hence, the flight data show a more outboard position for the spanwise center-of-pressure location than do the wind tunnel or theoretical data, particularly for the transonic Mach numbers where the leading edge is most highly loaded.

Transonically, the flight data show that the chordwise center of pressure moves from 22 percent of the MAC at Mach 0.70 to 10 percent of the MAC at Mach 0.95. The wind tunnel data show a similar trend with Mach number, but indicate that the center of pressure is located slightly farther aft.

The theory shows a forward located center of pressure at about 14 percent of the MAC but predicts little movement in the center of pressure with changes in Mach number. The forward moving location of the chordwise center of pressure contrasts with the center-of-pressure movement for higher-aspect-ratio planforms. This could have a significant impact on the structural design of very low-aspect-ratio lifting surfaces. Supersonically, the chordwise center-of-pressure location moves aft and approaches 50 percent of the MAC at Mach 2.

Figure 10 shows the aileron crossflow loads which were obtained from aileron pulse maneuvers. At Mach numbers of 0.98 and above, aileron deflections do not affect the ventral fin loads; however, for transonic Mach numbers less than 0.98, aileron deflections do affect the ventral fin loads, most notably the torque loads,  $C_{T\delta_a}$ . Transonically,  $C_{N\delta_a}$  and  $C_{B\delta_a}$  are fairly constant with change in Mach number, but  $C_{T\delta_a}$  varies in level from -0.0016 at Mach 0.7 to -0.0027 at Mach 0.95.

Although the effects of  $C_{N\delta_a}$  and  $C_{B\delta_a}$  are small or even negligible when compared with the loads imposed on the ventral fin from sideslip (figs. 8 and 9), torque loads due to aileron deflection,  $C_{T\delta_a}$ , are significant when compared with torque loads

due to sideslip,  $C_{T\beta}$ . The wind tunnel data show good agreement with the flight data, and the theoretical calculations at Mach 0.90 show good agreement with the flight data for  $C_{T\delta_a}$  but overestimate  $C_{N\delta_a}$  and  $C_{B\delta_a}$ . The discrepancies may be attributed to the idealization of the airplane's configuration for computer modeling in the linear aerodynamic theory.

## CONCLUDING REMARKS

The aerodynamic loads of a 0.92-aspect-ratio ventral fin were measured during a flight test program of the YF-12A airplane. These data, which cover the Mach number range from 0.70 to 2.00, are presented in coefficient form and are compared with data obtained from wind tunnel tests and with the results obtained from application of a linear aerodynamic theory.

The loads induced on the ventral fin were found to result from (1) the load due to change in the angle of sideslip and (2) the load due to aileron deflection because of the proximity of the fin to the ailerons.

The flight data show that the slope of the normal force curve peaks at a Mach number of about 1.2 to 1.4 instead of about Mach 1.0, as is the case with slightly higher aspect-ratio planforms. Also, as the Mach number increases transonically, the chordwise center-of-pressure location moves forward from 22 percent of the MAC at Mach 0.7 to 10 percent of the MAC at Mach 0.95 before moving aft as Mach number increases supersonically.

Wind tunnel and flight pressure data suggest the presence of a leading edge vortex which adds an increment of load to the ventral fin and which results in a nonlinear normal force curve.

The wind tunnel data and theoretical calculations were in fair agreement with the flight data although the data from the theoretical calculations were not as sensitive to change in Mach number as were the flight-measured data and the wind tunnel data.

The deflection of the ailerons affected the ventral fin loads up to a Mach number of 0.98. Although aileron deflections had little effect on the normal force and bending moment coefficients, they had a pronounced effect on the torque coefficient since the aileron crossflow load was concentrated on the aft portion of the fin. At airspeeds greater than Mach 0.98 there were no aileron-induced loads on the ventral fin.

The forward center-of-pressure location of the additional airload could influence the structural design of very low-aspect-ratio lifting surfaces, and the combination of the additional airload and the aileron crossflow loads could result in large torque loads on this type of fin.

## REFERENCES

1. Keener, Earl R.; and Jordan, Gareth H.: Wing Loads and Load Distributions Throughout the Lift Range of the Douglas X-3 Research Airplane at Transonic Speeds. NACA RM H56G13, 1956.
2. Pyle, Jon S.: Flight-Measured Wing Surface Pressures and Loads for the X-15 Airplane at Mach Numbers From 1.2 to 6.0. NASA TN D-2602, 1965.
3. Jenkins, Jerald M.; DeAngelis, V. Michael; Friend, Edward L.; and Monaghan, Richard C.: Flight Measurements of Canard Loads, Canard Buffeting, and Elevon and Wing-Tip Hinge Moments on the XB-70 Aircraft Including Comparisons With Predictions. NASA TN D-5359, 1969.
4. Mechtly, E. A.: The International System of Units - Physical Constants and Conversion Factors. Second Revision. NASA SP-7012, 1973.
5. Skopinski, T. H.; Aiken, William S., Jr.; and Huston, Wilber B.: Calibration of Strain-Gage Installations in Aircraft Structures for the Measurement of Flight Loads. NACA Rept. 1178, 1954.
6. Larson, Terry J.: Compensated and Uncompensated Nose Boom Static Pressures Measured From Two Air Data Systems on a Supersonic Airplane. NASA TM X-3132, 1974.
7. Dusto, A. R.; Brune, G. W.; Dornfeld, G. M.; Mercer, J. E.; Pilet, S. C.; Rubbert, P. E.; Schwanz, R. C.; Smutny, P.; Tinoco, E. N.; and Weber, J. A.: A Method for Predicting the Stability Characteristics of an Elastic Airplane. Volume 1-FLEXSTAB Theoretical Description. NASA CR-114712, 1974.
8. Woodward, F. A.; Tinoco, E. N.; and Larsen, J. W.: Analysis and Design of Supersonic Wing-Body Combinations, Including Flow Properties in Near Field. Part I: Theory and Application. NASA CR-73106, 1967.
9. LaRowe, E.; and Love, J. E.: Analysis and Design of Supersonic Wing-Body Combinations, Including Flow Properties in Near Field. Part II: Digital Computer Program Description. NASA CR-73107, 1967.

TABLE 1. — YF-12A FLIGHT INSTRUMENTATION ACCURACY

Parameter	Estimated accuracy
Mach number	
Supersonic . . . . .	± 0.012
Subsonic . . . . .	± 0.004
Airspeed, m/sec	
Supersonic . . . . .	± 0.3
Subsonic . . . . .	± 0.5
Altitude, m	
Subsonic, supersonic . . . . .	± 46
Transonic . . . . .	± 67
Dynamic pressure, N/m <sup>2</sup>	
Supersonic . . . . .	± 72
Subsonic . . . . .	± 287
Angle of attack, deg	
Subsonic, supersonic . . . . .	± 0.25
Transonic . . . . .	± 0.50
Angle of sideslip, deg . . . . .	± 0.25
Elevon position, deg . . . . .	± 0.1
Fuel quantities, N . . . . .	± 1334
Accelerations, g	
Vertical . . . . .	± 0.04
Lateral . . . . .	± 0.01
Longitudinal . . . . .	± 0.06
Attitudes, deg	
Pitch . . . . .	± 0.4
Roll . . . . .	± 1.2
Yaw . . . . .	± 0.4
Rates, deg/sec	
Pitch . . . . .	± 0.1
Roll . . . . .	± 0.1
Yaw . . . . .	± 0.1
Pressure coefficient . . . . .	± 0.01
Normal force coefficient, percent . . . . .	5
Bending moment coefficient, percent . . . . .	15
Torque coefficient, percent . . . . .	8

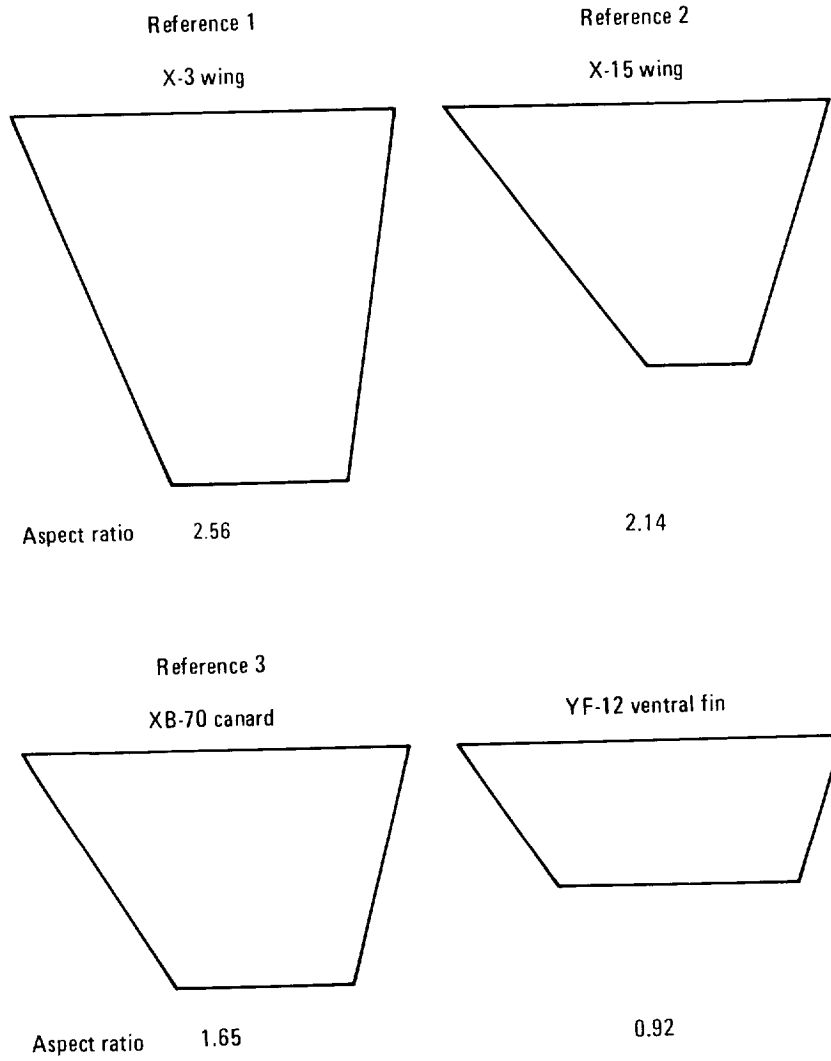


Figure 1.—Some low-aspect-ratio lifting surfaces for which experimental aerodynamic loads data are available. Planforms not drawn to scale.

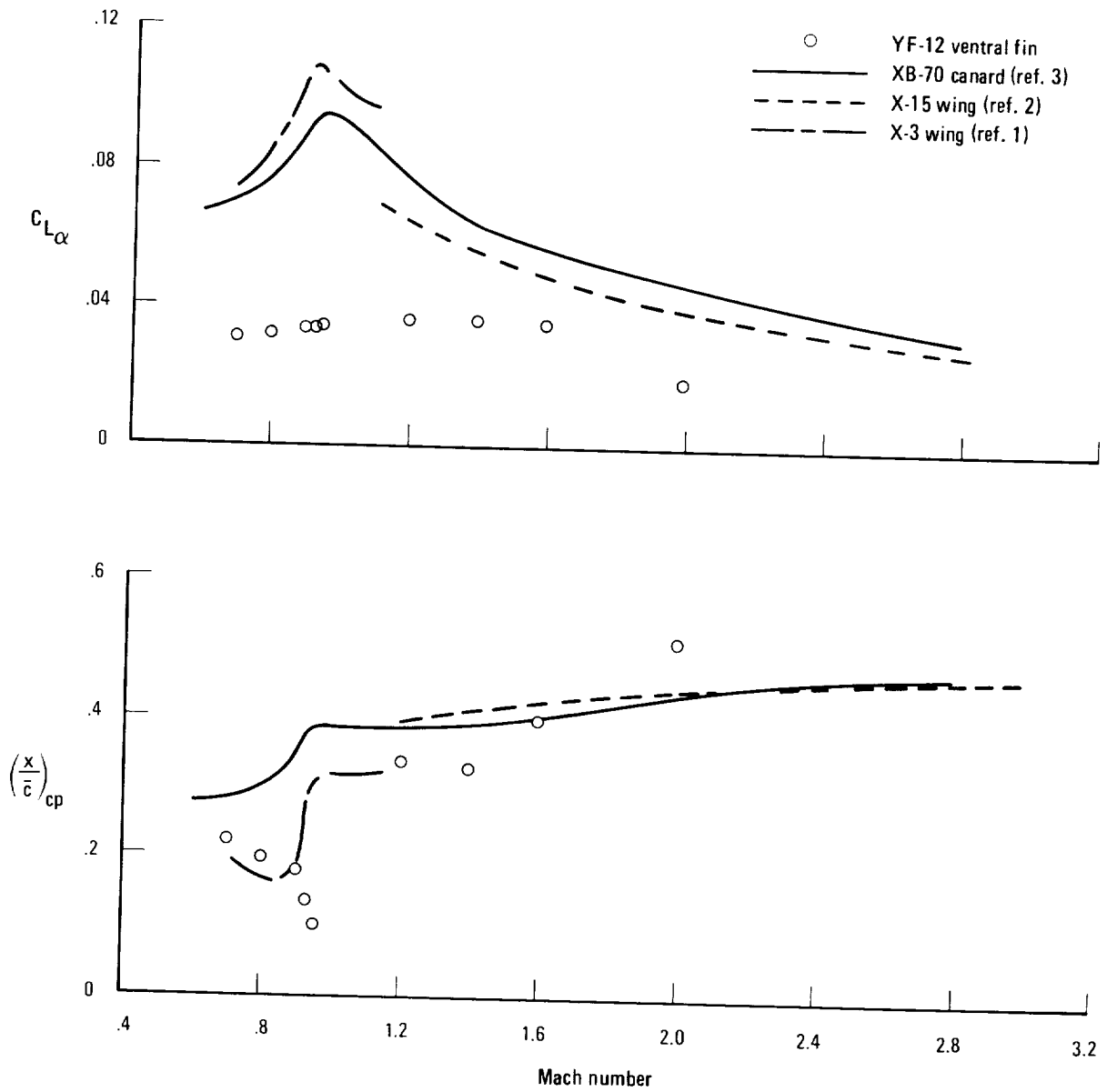


Figure 2.—Variation of flight-determined lift curve slope and chordwise center-of-pressure location with Mach number for several low-aspect-ratio lifting surfaces.

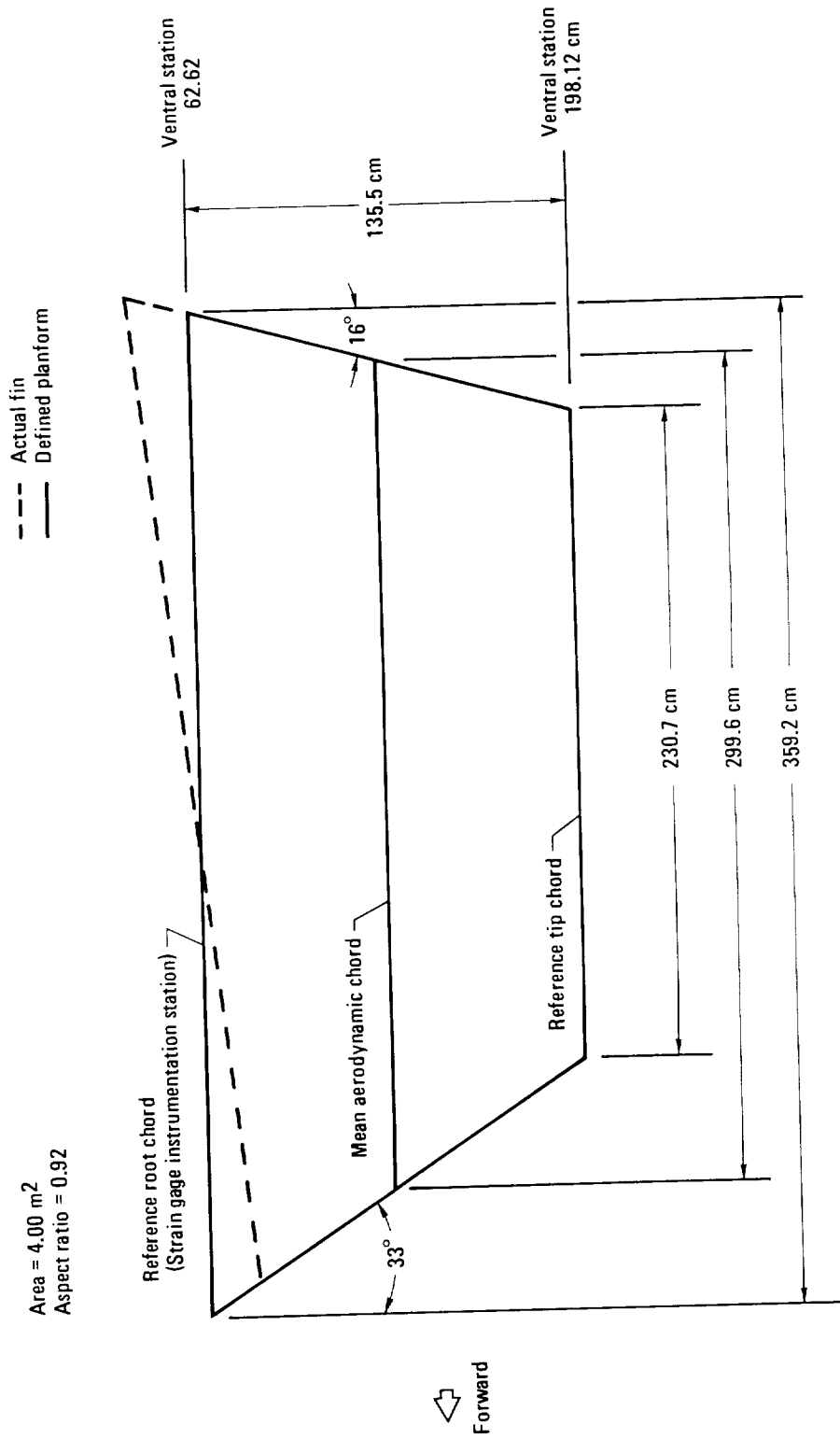


Figure 3.—Defined planform of flight test ventral fin, YF-12A airplane.

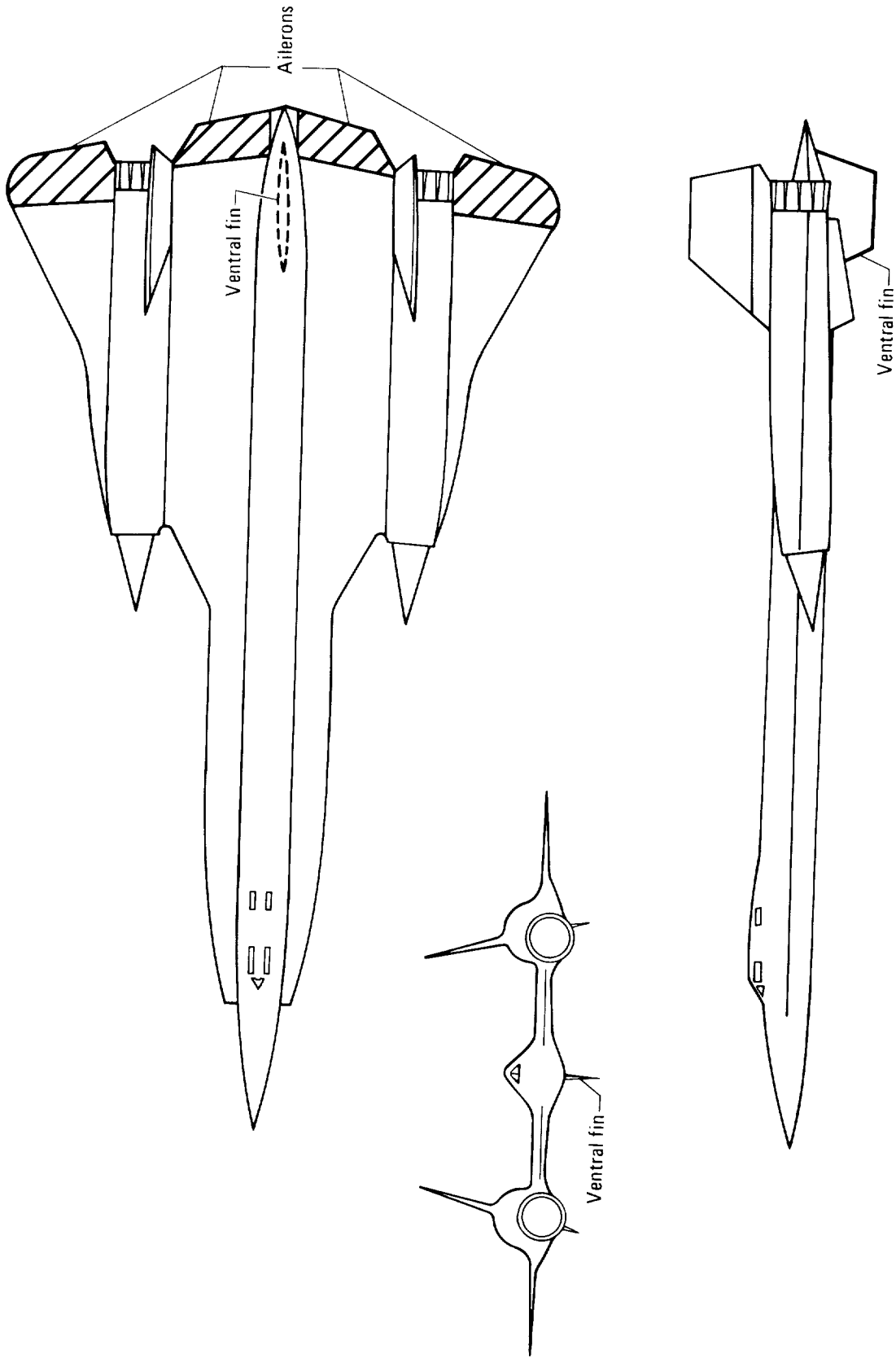


Figure 4.—Three views of YF-12A airplane showing proximity of ailerons to ventral fin.

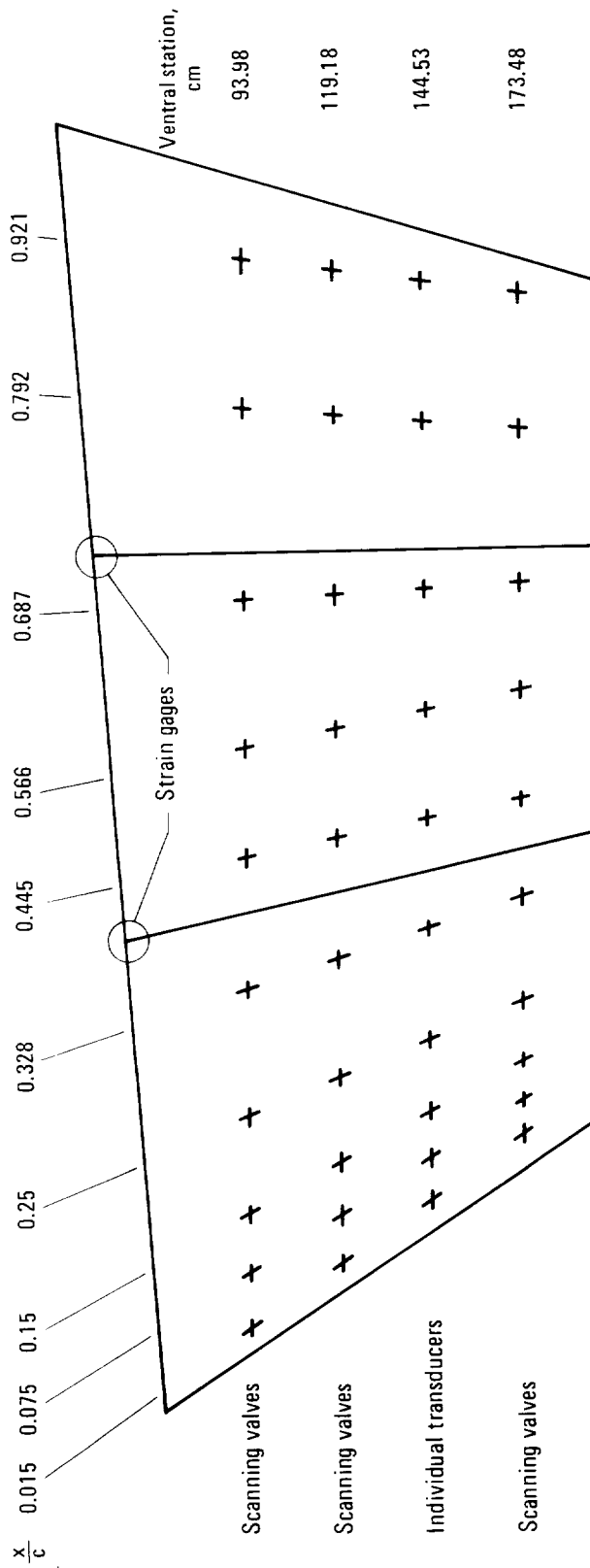


Figure 5.—Ventral fin instrumentation.

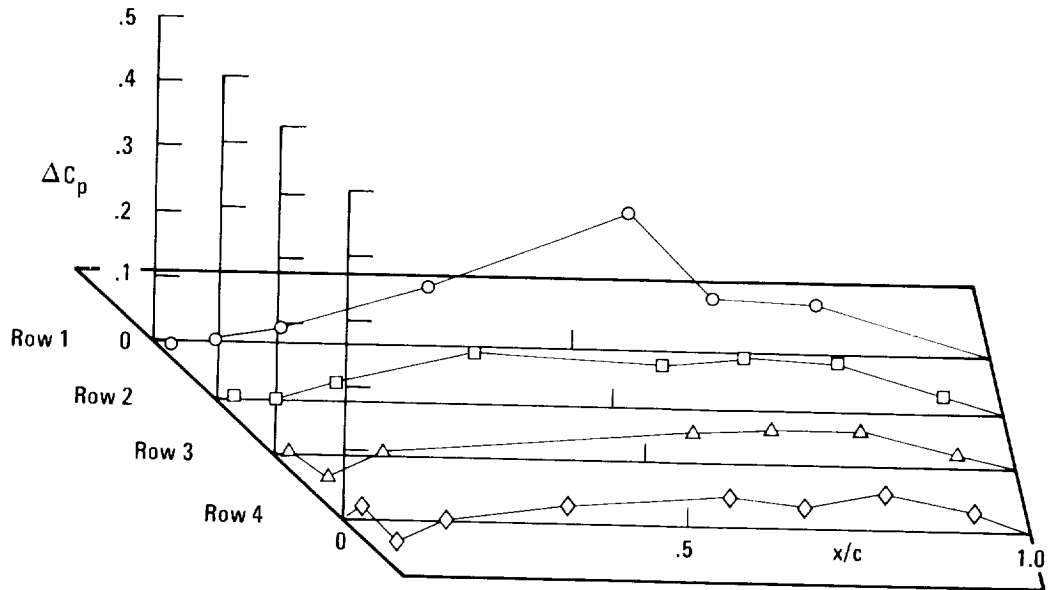


Figure 6.—Wind tunnel pressure distribution on ventral fin due to aileron deflection.  $M = 0.90$ ,  $\delta_a = 10^\circ$ ,  $\beta = 0^\circ$ .

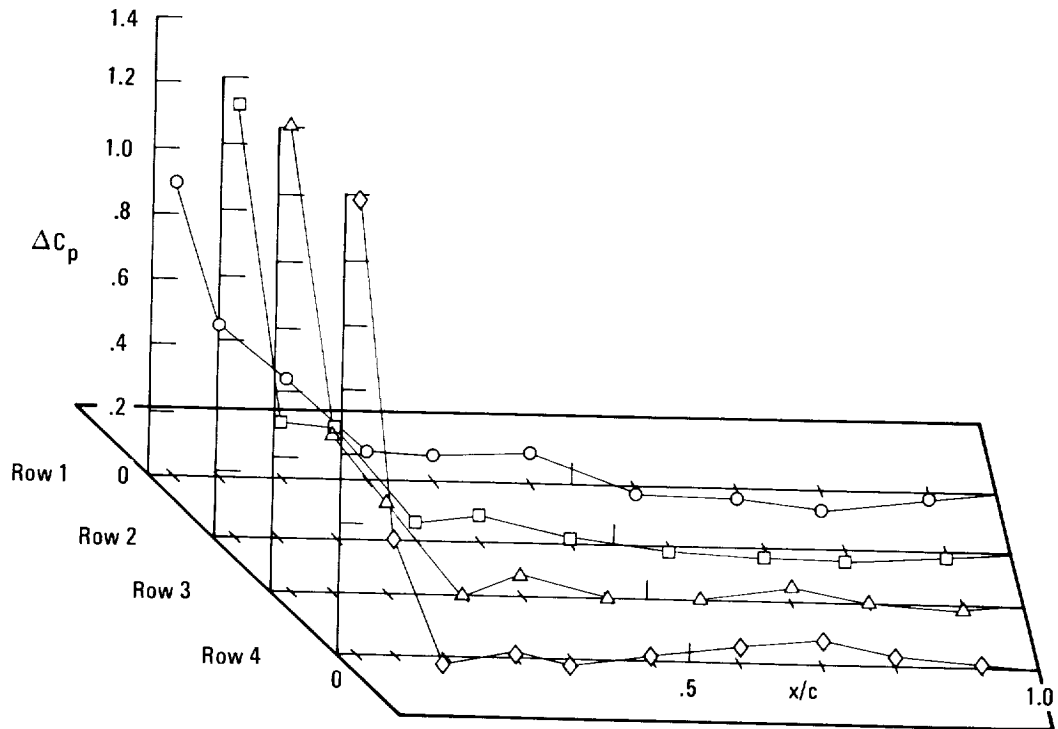


Figure 7.—Flight-measured pressure distribution on ventral fin due to steady-state sideslip loads.  $M = 0.90$ ,  $\delta_a = 3.7^\circ$ ,  $\beta = -3.8^\circ$ .

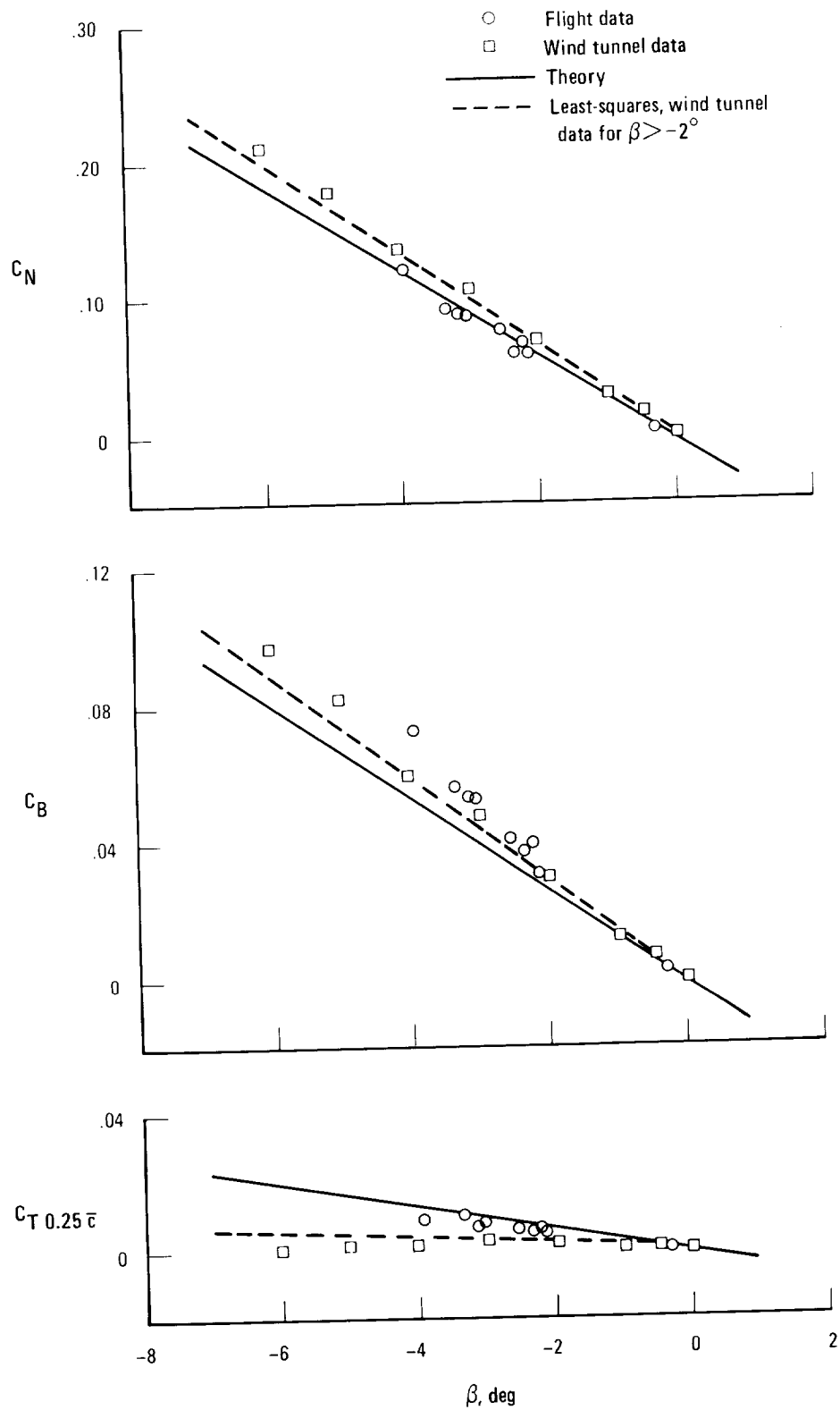


Figure 8.—Ventral fin load coefficients for flight, wind tunnel, and theoretical data shown as a function of angle of sideslip at Mach 0.90.

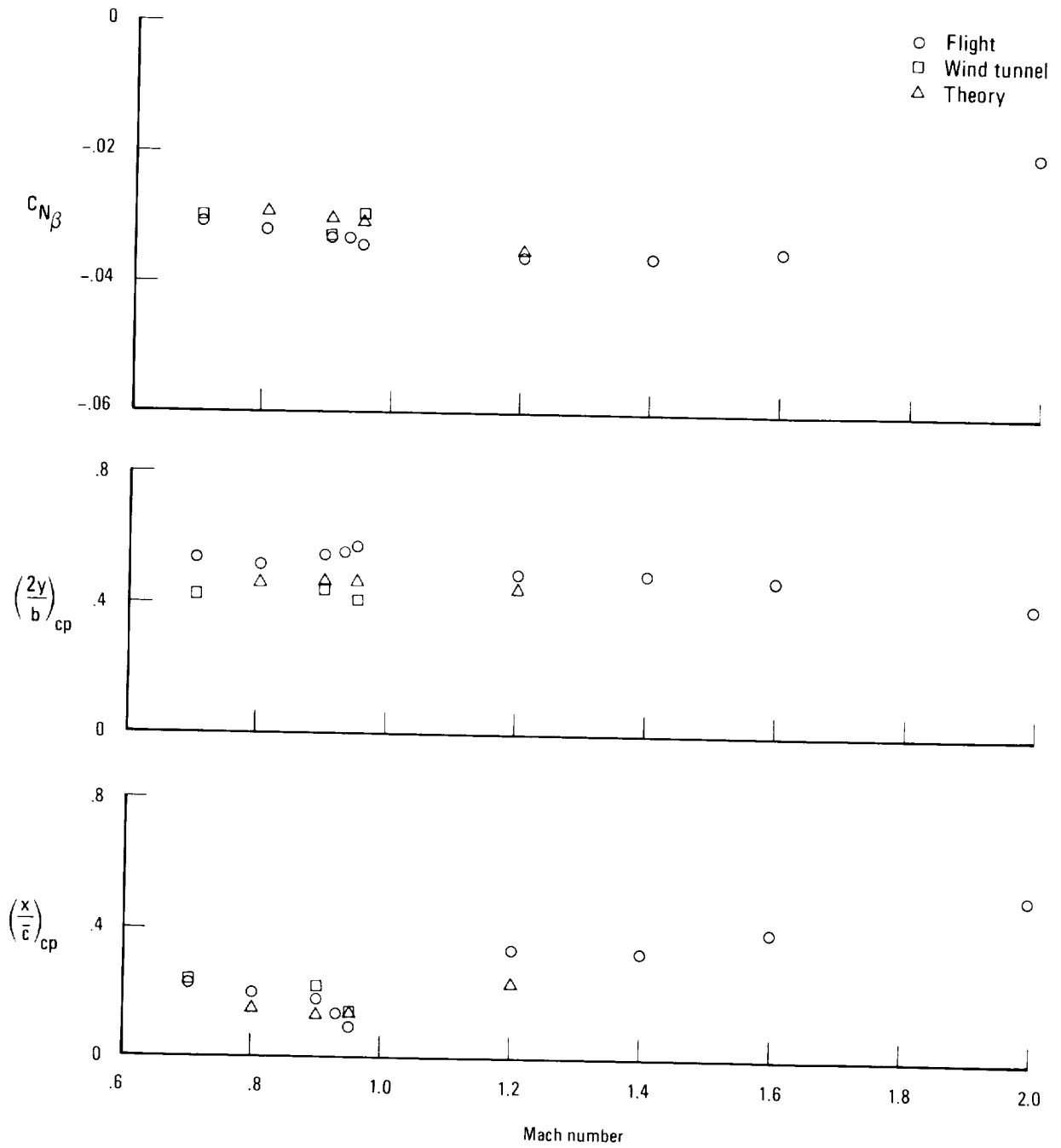


Figure 9.—Variation of ventral fin normal force coefficient slopes and center-of-pressure locations with Mach number.

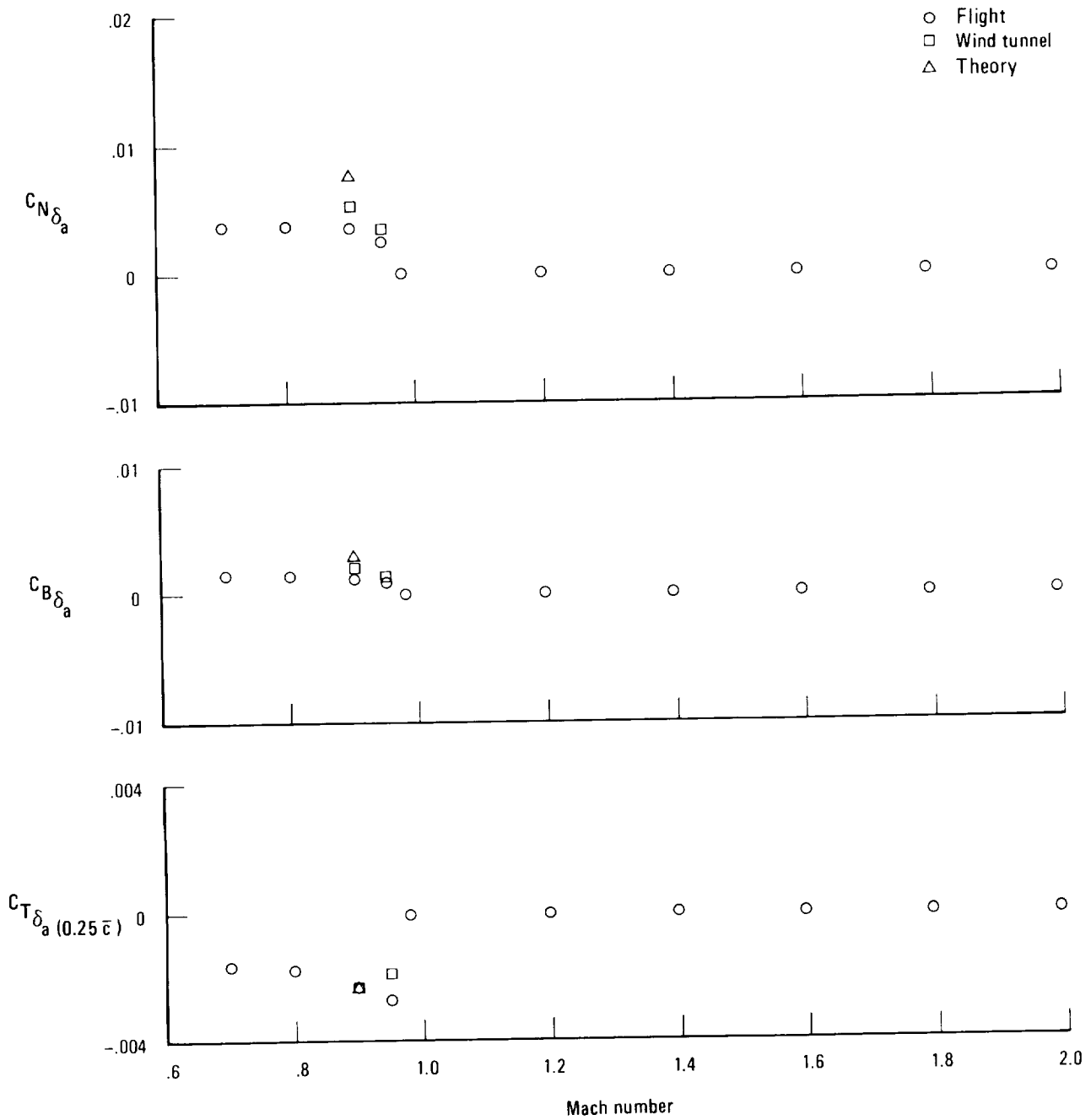


Figure 10.—Variation of ventral fin load coefficients due to aileron deflection with Mach number.